

Charge and Spin Dynamics and Enantioselectivity in Chiral Molecules

J. Fransson*

Department of Physics and Astronomy, Box 516, 751 21, Uppsala University, Uppsala, SWEDEN

(Dated: March 7, 2022)

Charge and spin dynamics is addressed in chiral molecules immediately after the instantaneous coupling to an external metallic reservoir. It is shown how a spin-polarization is induced in the chiral structure as a response to the charge dynamics. The dynamics indicate that chiral induced spin selectivity is an excited states phenomenon which, in the transient regime partly can be captured using a simplistic single particle description, however, in the stationary limit definitively shows that electron correlations, e.g., electron-vibration interactions, crucially contribute to sustain an intrinsic spin anisotropy that can lead to a non-vanishing spin selectivity. The dynamics, moreover, provide insight to enantiomer separation, due to different acquired spin-polarizations.

During the course of more than the past two decades, we have learnt that electron spin selective processes are intimately associated with chirality [1, 2]. The effect can partly be understood as emerging from a combination of structural chirality, spin-orbit interactions, and non-equilibrium conditions [3–28]. Nevertheless, despite that non-equilibrium conditions, which define the measurements, for instance, light exposure [1, 2, 31–35], local probing techniques [36–39], transport [37, 40, 41] and different types of Hall measurements [32, 33, 42–44], many theoretical accounts of the effect are based on the transmission properties of chiral molecules embedded in a given environment [3–8, 10–13, 15–17, 19, 20]. While the transmission pertains to the linear response regime, hence, the ground state properties of the molecule, it is also often typically the result of a single particle description which under stationary condition cannot account for the excited states properties that underly spin selectivity in chiral molecules.

Recent theoretical developments very clearly point towards the necessity to consider chiral induced spin selectivity from an excited states point of view [18, 21–23, 25–30], stressing the vital role of electronic correlations. It was shown that, e.g., Coulomb [18, 25, 29] and electron-vibration [21, 23, 24, 30] interactions, as well as polarons [22], photoexcitations [26], time-dependence [27], and dissipation [28] generate the exchange necessary to create measurable effects regarding chiral induced spin selectivity.

In this context, an obvious question is how a spin-polarization can be generated and stabilized in a molecular structure which is in a closed shell configuration when isolated from the surrounding environment. Recent experiments demonstrate that a measurable spin-polarization can be obtained whenever chiral molecules are interfaced with metallic surfaces [42, 45–47]. Through the anomalous Hall effect, chiral molecules were, for instance, shown to control the magnetism in thin Co layers [42, 45] and enantiomer separation on non-magnetic metals [46], whereas Yu-Shiba-Rusinov states [48–50] were observed in the vicinity of chiral molecules on the surface of superconducting NbSe₂ [47]. Related to these observations are also the results showing strongly enantiomer dependent binding energies on ferromagnetic metals [51–56]. Theoretically, enantiomer separation was addressed in Refs. 29, 30 for molecules in contact with ferromagnetic

metal, based on descriptions in which the effective electronic exchange plays a crucial role in the magnetic response. On the other hand, while excited states appear to be crucial, the question of how spin-polarization emerges in chiral molecules when in contacted with a metal remains open.

In this Letter, it is shown that a finite spin-polarization is dynamically generated in chiral molecules as a response to the charge dynamics when interfaced with a metal. The dynamics indicate that chiral induced spin selectivity is an excited states phenomenon which, in the transient regime partly can be captured using a simplistic single particle description, while such a description is not sufficient in the stationary limit. The latter statement is founded on that the spin-polarization eventually vanishes which, in turns, implies that any mechanism that can sustain an immanent spin anisotropy has to account for excited states properties, e.g., electron-electron or electron-vibration interactions. In the subsequent discussion it is, therefore, shown that, by adding electron-vibration interactions in the adiabatic limit, the transient spin fluctuations are stabilized and developed into a finite stationary spin-polarization. Finally, when interfacing the different enantiomers on ferromagnet, the results presented herein provide fundamental clues for a comprehensive picture of enantiomer separation.

The presented discussion is based on simulations of idealized chiral models of realistic, e.g., α -helix, oligopeptides, and polyanilines. In this context the specific details of the molecules strongly vary, however, the salient properties such as chirality, spin-orbit interaction, and interface to a metal are captured. The model was previously proposed in order to point out the importance of electronic correlations originating from Coulomb [18] and electron-vibration [23, 30] interactions. Here, such mechanisms are first excluded for sake of highlighting the dynamics of excited states as a fundamental component in the charge redistribution and accompanied spin-polarization immediately after interfacing the molecule with the metal. Then, in the subsequent discussion it is shown that electron-vibration interactions stabilize a non-vanishing spin-polarizations also in the stationary limit, hence, emphasizing that the phenomenon of chiral induced spin selectivity is an excited states effect.

The simulations are based on a model of a chiral structure comprising a set of $\mathbb{M} = M \times N$ nuclear coordinates $\mathbf{r}_m = (a \cos \varphi_m, a \sin \varphi_m, c_m)$, $\varphi_m = 2\pi(m-1)/(\mathbb{M}-1)$, and $c_m =$

$c\varphi_m/2\pi$, where a and c define the radius and length, respectively, of the helix of M laps and N nuclei per lap. The molecule is described by the single-electron levels $\varepsilon = \text{diag}\{\varepsilon_1, \varepsilon_2, \dots, \varepsilon_M\}$, representing the energy levels at \mathbf{r}_m , associated with the electron creation and annihilation spinors ψ_m^\dagger and ψ_m , respectively. Nearest neighbors interact via elastic and inelastic hopping with rates t_0 and t_1 , respectively, while next-nearest neighbors interact via the effective static and non-static spin-orbit interaction with rates λ_0 and λ_1 , through processes of the type $i\psi_m^\dagger \mathbf{v}_m^{(s)} \cdot \boldsymbol{\sigma} \psi_{m+2s}$, $s = \pm 1$, where $\mathbf{v}_m^{(s)} = \hat{\mathbf{d}}_{m+s} \times \hat{\mathbf{d}}_{m+2s}$, defines the chirality in terms of the unit vectors $\hat{\mathbf{d}}_{m+s} = (\mathbf{r}_m - \mathbf{r}_{m+s})/|\mathbf{r}_m - \mathbf{r}_{m+s}|$, such that different enantiomers are represented by the sign (\pm) of the chirality. The notation σ^0 and $\boldsymbol{\sigma}$ refer to the identity and vector of Pauli matrices, respectively. The nuclear, or, molecular vibrations are captured in the coherent vibrational mode ω_0 , which is created and annihilated by the phonon operators b^\dagger and b , respectively. A Hamiltonian model can be written $\mathcal{H}_{\text{mol}} = \mathcal{H}_0 + \mathcal{H}_1 = \Psi^\dagger [\mathbf{H}_0 + \mathbf{H}_1(b + b^\dagger)] \Psi$, where $\Psi = (\psi_1, \psi_2, \dots, \psi_M)^T$ and

$$\mathcal{H}_0 = \sum_{m=1}^M \varepsilon_m \psi_m^\dagger \psi_m + \omega_0 b^\dagger b - t_0 \sum_{m=1}^{M-1} (\psi_m^\dagger \psi_{m+1} + H.c.) + \lambda_0 \sum_{m=1}^{M-2} (i\psi_m^\dagger \mathbf{v}_m^{(+)} \cdot \boldsymbol{\sigma} \psi_{m+2} + H.c.), \quad (1a)$$

$$\mathcal{H}_1 = -t_1 \sum_{m=1}^{M-1} (\psi_m^\dagger \psi_{m+1} + H.c.)(b + b^\dagger) + \lambda_1 \sum_{m=1}^{M-2} (i\psi_m^\dagger \mathbf{v}_m^{(+)} \cdot \boldsymbol{\sigma} \psi_{m+2} + H.c.)(b + b^\dagger). \quad (1b)$$

The properties of the metal to which the molecule is connected are captured by the parameters $\Gamma = \Gamma(\sigma^0 + p\sigma^z)/2$, representing the coupling between the nuclear site 1 and the metal. Here, $\Gamma = 2\pi \sum_{\mathbf{k}\sigma} |\nu_{\mathbf{k}\sigma}|^2 \rho_\sigma(\varepsilon_{\mathbf{k}})$ accounts for the spin-dependent hybridization $\nu_{\mathbf{k}\sigma}$ and spin-density $\rho_\sigma(\varepsilon_{\mathbf{k}})$ of the electrons in the metal, whereas $|p| \leq 1$ denotes the effective spin-polarization of the coupling.

The time-evolution of the electronic structure of the molecule can be related to the time-dependent Green function $\mathbf{G}_{mm}(t, t') = (-i)\langle T\psi_m(t)\psi_m^\dagger(t') \rangle$ through, e.g., the charge $\langle n_m(t) \rangle = (-i)\text{sp}\mathbf{G}_{mm}^<(t, t)$ and spin-moment $\langle \mathbf{s}(t) \rangle = (-i)\text{sp}\boldsymbol{\sigma}\mathbf{G}_{mm}^<(t, t)/2$, where $\mathbf{G}^{</>}(t, t')$ is proportional to the density of occupied/unoccupied electron states. Here, sp denotes the trace over spin 1/2 space.

As the main interest here lies on the time-dependence of the molecular properties immediately after the time t_0 when the molecule is interfaced with the metal, the interaction with the metal is treated with a time-dependent hybridization $\nu_{\mathbf{k}\sigma}(t) = \nu_{\mathbf{k}\sigma}\theta(t - t_0)$, where $\theta(t)$ is the Heaviside step function. In the view of this time-dependent interaction, the equation of motion for the static ($\mathbf{H}_1 = 0$) Green function can be written

as the Dyson equation

$$\mathbf{G}(t, t')d\tau = \mathbf{g}(t, t') + \int \mathbf{g}(t, \tau)\boldsymbol{\Sigma}(\tau, \tau')\mathbf{G}(\tau', t')d\tau d\tau', \quad (2a)$$

$$\boldsymbol{\Sigma}(t, t') = \sum_{\mathbf{k}} \mathbf{v}_{\mathbf{k}}(t)\mathbf{g}_{\mathbf{k}}(t, \tau)\mathbf{v}_{\mathbf{k}}^\dagger(t'). \quad (2b)$$

The bare Green functions $\mathbf{g}(t, t') = (-i)T e^{-i\mathbf{H}_0(t-t')}$ and $\mathbf{g}_{\mathbf{k}}(t, t') = (-i)T \sigma^0 e^{-i\varepsilon_{\mathbf{k}}(t-t')}$ carry trivial time-dependencies, and alluding to the wide band limit for the electronic band in the metal [57], the lesser self-energy can be simplified into

$$\boldsymbol{\Sigma}^<(t, t') = i\Gamma\theta(t - t_0)\theta(t' - t_0) \int f(\omega) e^{-i\omega(t-t')} \frac{d\omega}{2\pi}, \quad (3)$$

where $f(\omega) = f(\omega - \mu)$ is the Fermi-Dirac distribution function defined at the chemical potential μ of the metal. Thanks to this simplification, and the relation $\mathbf{G}^< = \mathbf{G}^r \boldsymbol{\Sigma}^< \mathbf{G}^a$, where $\mathbf{G}^{r/a}$ is the retarded/advanced Green function, the dressed lesser and retarded/advanced Green functions for the molecule becomes

$$\mathbf{G}^<(t, t') = i \int_{t_0}^{\infty} f(\omega) \mathbf{G}^r(t, \tau) \Gamma \mathbf{G}^a(\tau', t') e^{-i\omega(\tau - \tau')} d\tau d\tau', \quad (4a)$$

$$\mathbf{G}^{r/a}(t, t') = (\mp i)\theta(\pm t \mp t') e^{-i\mathbf{H}_0(t-t') \mp \Gamma(t, t')/2}, \quad (4b)$$

where the expression in Eq. (4a) is valid for $t, t' > t_0$, whereas $\Gamma(t, t') = \Gamma \int_{t_0}^t \theta(s - t_0) ds$.

Effects from inelastic scattering are included by repeating Eq. (2a), defining a dressed Green function \mathbb{G} and self-energy $\boldsymbol{\Sigma}_{\text{vib}}(t, t') = i\mathbf{H}_1 \mathbf{g}(t, t') d(t, t') \mathbf{H}_1$, where $d(t, t') = 2T \sin \omega_0(t - t')$ is the propagator for the nuclear vibrations. However, since the aim is to provide a simple description of the charge and spin dynamics and a mechanism which eventually leads to a non-vanishing spin-polarized stationary state, as discussed in Ref. 30, the full Dyson equation for \mathbb{G} is reduced to the adiabatic (Markovian) approximation, in which the self-energy becomes time-independent. In this form, the resulting retarded Green function can be written on the form

$$\mathbb{G}^r(t, t') = (-i)\theta(t - t') e^{-i(\mathbf{H}_0 + \boldsymbol{\Sigma}_{\text{vib}})(t-t') \mp \Gamma(t, t')/2}, \quad (5)$$

in which expression $\boldsymbol{\Sigma}_{\text{vib}} = \mathbf{H}_1 \mathbf{L} \mathbf{H}_1$, where \mathbf{L} is a diagonal matrix where the entries are defined by the electron-phonon loop

$$L_{mm} = \frac{n_B(\omega_0) + 1 - f(\varepsilon_m)}{\varepsilon_m + \omega_0 - i/\tau_{\text{ph}}} + \frac{n_B(\omega_0) + f(\varepsilon_m)}{\varepsilon_m - \omega_0 - i/\tau_{\text{ph}}}, \quad (6)$$

and $n_B(\omega)$ is the Bose-Einstein distribution function, whereas τ_{ph} defines an intrinsic vibrational life-time.

In a previous discussion, it was shown that the molecular structure given in \mathbf{H}_0 , Eq. (1a), carries necessary components that lift the spin-degeneracy, arising from a confluence of the spin-orbit interactions and the chiral geometry [18]. However, the structure has to include at least four nuclear sites and be under non-equilibrium conditions, of which

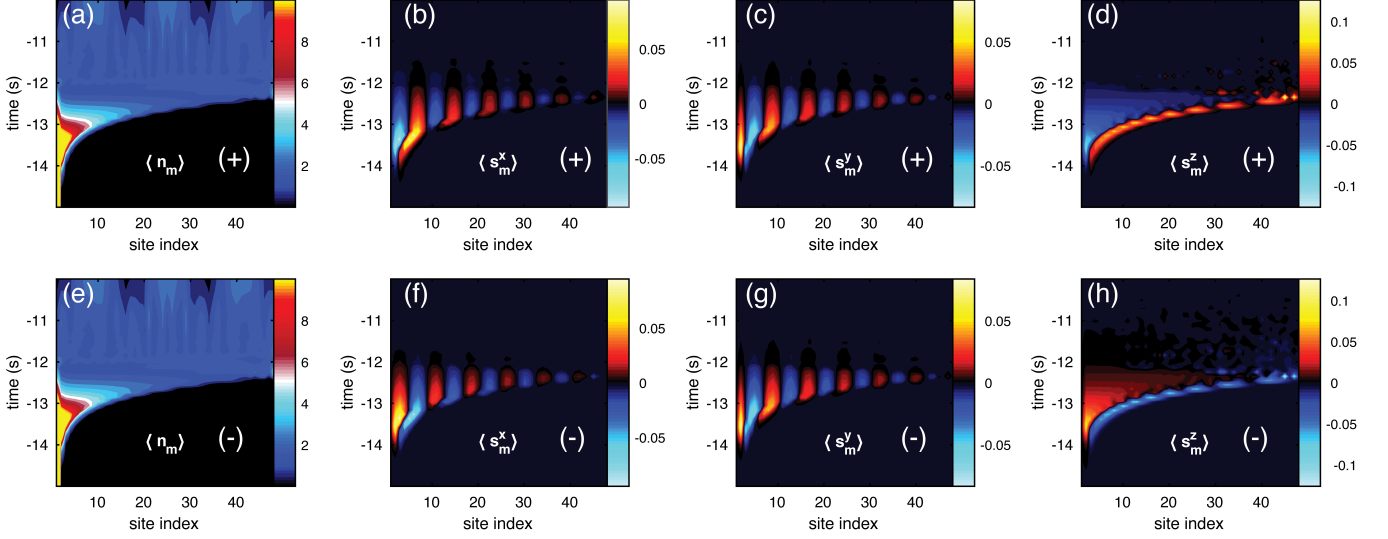


FIG. 1. Single electron picture of the charge and spin dynamics in a chiral molecule (6×8) after making instantaneous contact with a metal. The spatially resolved charge $\langle n_m \rangle$ (a), (e), and spin projections $\langle s_m^x \rangle$ (b), (f), $\langle s_m^y \rangle$ (c), (g), $\langle s_m^z \rangle$ (d), (h), are simulated for positive (+) (a) – (d) and negative (–) (e) – (h) helicity. Parameters used are $a = 5 \text{ \AA}$, $c = 235 \text{ \AA}$, $\epsilon_m - \mu_L = -2$, $\lambda_0 = 1/40$, and $\Gamma^L = 1/4$, in units of $t_0 = 40 \text{ meV}$, simulated at $T = 300 \text{ K}$. Time given on a logarithmic scale.

the latter was previously considered to be arising from external voltage bias applied across a junction between metallic leads in which the molecule was mounted. The lack of a coupling between the internal and dissipative degrees of freedom does, nonetheless, not allow the structure to maintain a stationary spin-polarization when mounted with only one end to a metal and held in equilibrium, see Ref. 30. Such a mechanism is provided by the coupling between electronic and vibrational degrees of freedom in \mathbf{H}_1 , Eq. (1b). Hence, in the present discussion, it will be shown that the elastic spectrum provided through \mathbf{H}_0 can only be used to capture strictly non-equilibrium properties, while the stationary properties are maintained by inclusion of also \mathbf{H}_1 . The discussion makes it is clear that while electron correlations have to be included for an adequate description, the simplified single electron picture does provide crucial insight into the emergence of the spin symmetry breaking.

In terms of the presented model, Eq. (1), the magnetic moment of the molecule vanishes whenever the molecule is isolated from the metallic environment. At the time instant when the molecule is attached to the metal, the molecule is set into a strongly non-equilibrium state where electrons are passing through the interface between the molecule and metal, rendering a redistribution of charge in the molecule. These processes are captured very well already at the single electron level ($\mathbf{H}_1 = 0$), see Fig. 1 (a), (e), where a spatially resolved time-evolution of the molecular charge, $\langle n_m \rangle$, is shown for a (6×8 sites) chiral molecule with (a) positive and (e) negative chirality immediately after the instantaneous attachment of the molecule to a normal metal. In addition to showing that the time-evolution of the charge distribution is the same in the

two enantiomers, the plots also show the strong fluctuations of the charge due to the abrupt changes in the environment of the molecules.

As a result of the charge motion in the chiral molecule, an accompanied spin-polarization emerges and evolves both in time and space, see Fig. 1 (b)–(d), (f)–(h), showing the projections of $\langle s_m \rangle$ for the two enantiomers. While the plots appear to suggest the opposite, the spin redistribution also responds instantaneously when contacting the molecule with the metal, however, there is a time delay (about 10 fs in the example) before the accumulated spin angular momentum becomes sufficiently large to be visible on the given scale. The plots, moreover, illustrate that there is a finite time frame during which the spin-polarization is significant, after which it vanes and eventually vanishes (around 1 ps after contact).

Concerning the spin-polarization, there are two distinctive features which are clearly illustrated in Fig. 1. First, the transverse projections, $\langle s_m^{x,y} \rangle$, indicate anti-ferromagnetic spin configurations resulting in no, or little, net moment perpendicular to the length direction of the molecule. This is in sharp contrast to the longitudinal projection $\langle s_m^z \rangle$, where the moment on each site first becomes positive (negative), then switches sign and eventually vanes, with the exception that the moments tend to switch once again at the sites near the free end of the molecule. Second, the two enantiomers acquire opposite spin-polarizations such that the spin moments $\langle s_m \rangle_{\pm} = (\langle s_m^x \rangle_{\pm}, \langle s_m^y \rangle_{\pm}, \langle s_m^z \rangle_{\pm})$ in the \pm enantiomers, respectively, are related by rotating the spins around the y-projection, that is, $(\langle s_m^x \rangle_{-}, \langle s_m^y \rangle_{-}, \langle s_m^z \rangle_{-}) = (-\langle s_m^x \rangle_{+}, \langle s_m^y \rangle_{+}, -\langle s_m^z \rangle_{+})$.

Inclusion of molecular vibrations changes the qualitative aspects of the charge and spin dynamics, see Fig. 2, showing

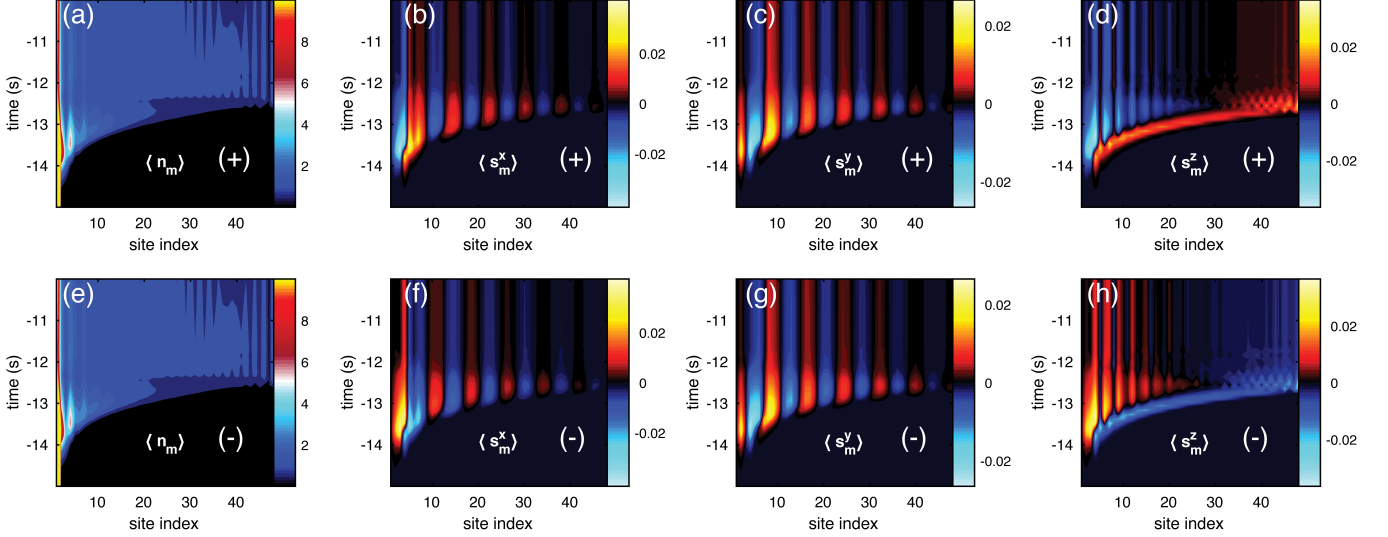


FIG. 2. Charge and spin dynamics in a vibrating chiral molecule (6×8) after making instantaneous contact with a metal. The spatially resolved charge $\langle n_m \rangle$ (a), (e), and spin projections $\langle s_m^x \rangle$ (b), (f), $\langle s_m^y \rangle$ (c), (g), $\langle s_m^z \rangle$ (d), (h), are simulated for positive (+) (a) – (d) and negative (–) (e) – (h) helicity. Parameters used are $t_1 = 1/10$, $\lambda_1 = 1/400$, and $1/\tau_{ph} = 1/4$, in units of $t_0 = 40$ meV, while other parameters are as in Fig. 1. Time given on a logarithmic scale.

the spatially resolved time-evolution of the molecular charge and spin from simulations with vibrating chiral molecules. First, it can be noticed that the vibrationally assisted spatial evolutions for both charge and spin initially are qualitatively similar to evolutions in the purely static molecule. However, while the charge in the static molecule returns to a more or less homogenous distribution in the stationary regime, after an initially strong accumulation near the interface to the metal, Fig. 1 (a), (e), in the vibrating molecule the accumulated charge near the interface is maintained also when the system has reached a stationary state, see Fig. 2 (a), (e). Second, it can be noticed that the spin-polarizations that develop shortly after contact with the metal, also remain when the system reaches a stationary state, Fig. 2 (b)–(d), (f)–(h). While the transverse projections are configured anti-ferromagnetically within the molecule, Fig. 2 (b), (c), (f), (g), the longitudinal projection finally reaches a spin-polarized state with opposite polarizations at the two ends of the molecule, Fig. 2 (d), (h). The stationary state that is eventually reached for the molecule, corroborates the results obtained in the stationary regime [30], albeit the two approximations used are not exactly equivalent. The consistency between the results, nonetheless, suggests that the dissipative component provides through the molecular vibrations should be realistic and sound.

While the property that the two enantiomers acquire opposite spin-polarization when in contact with the metal is expected, in the next step it will be shown that this feature also opens up for enantiomer separation. In experiments, this can be done by contacting the enantiomers on a ferromagnetic surface and measure, e.g. the absorption rate [51] or the force required to pull the molecule off the surface [54]. Here, the

enantiomer selectivity is studied through the magnetic properties of the composite system comprising both the molecule and the metal.

Using the spin-polarization as a tool for enantiomer separation was also considered in a recent theoretical study [58]. However, quantifying the enantiomer specific properties in terms of the transmission, which is essentially not a measurable quantity, introduces ambiguities in how to comprehend the results. The reason is that measurable quantities, such as the magnetic moment and charge current, are integrated over many degrees of freedom, in particular the energy dependencies of the involved mechanisms. Therefore, it is questionable whether the detailed spectral properties are meaningful in a context where such cannot be resolved.

Hence, here the enantiomer specific properties are investigated in terms of the mean spin-polarization $M^z = 2 \sum_m (z_m - \langle z \rangle) \langle s_m^z \rangle / a$, where $\langle z \rangle = \sum_m z_m / \mathbb{M}$, which defines a measure using which it is possible to determine whether there is any difference in the properties of the two enantiomers. As such, a negative (positive) spin-polarization can be understood as spin \uparrow (\downarrow) being accumulated towards the interface with the metal accompanied with a spin \uparrow (\downarrow) depletion towards the free end of the molecule. The advantage with this measure is that it directly connects to integrated measurable quantities such as the total magnetic moment since it provides a relation between the local magnetic moments $\langle s_m^z \rangle$ and the overall structure.

The mean spin-polarizations of static and vibrating molecules when in contact with a metal, are shown in Fig. 3. Bold (faint) lines in panels (a) and (b) correspond to simulations of the molecule in contact with a ferromagnetic (normal) metal with $p = 0.1$ ($p = 0$), while the plots in panel (c) shows

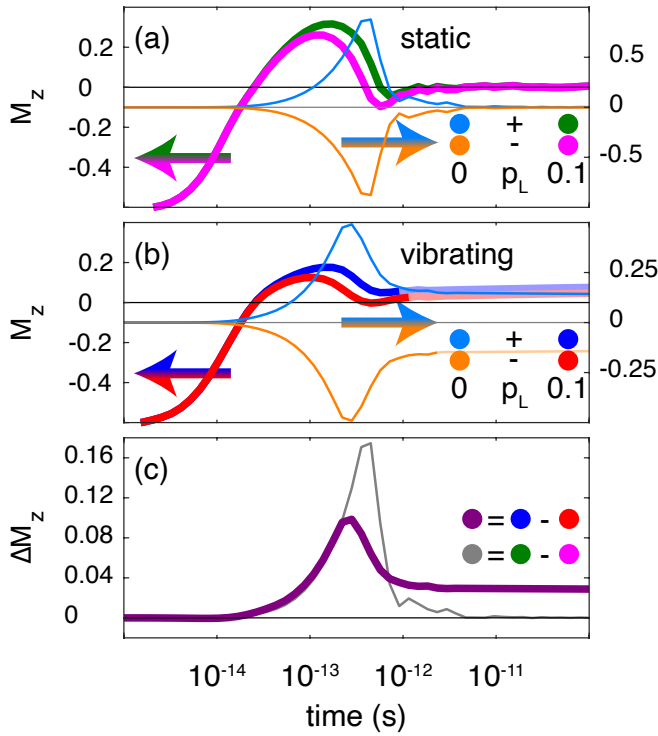


FIG. 3. Time evolution of mean spin-polarization M_z^\pm for (a) static molecule, (b) vibrating molecule, and (c) differences between the enantiomers ΔM_z in the static and vibrating configurations. Bold (faint) lines in panels (a) and (b) represent the results in presence of ferromagnetic (normal) metal with $p = 0.1$ ($p = 0$), for the two enantiomers \pm . In panel (c), the bold (faint) line represent the vibrating (static) configurations. Other parameters are as in Fig. 2.

the difference $\Delta M_z = M_z^+ - M_z^-$, where M_z^\pm denotes the spin polarization for the \pm enantiomers, for the vibrating (bold) and static (faint) configurations. Although the quantitative details vary between the static and vibrating configurations, the overall conclusion that can be drawn is that the enantiomers acquire different mean spin-polarizations, particularly in the transient regime. While the static configuration does not allow for a distinction between the enantiomers when reaching the stationary limit, the vibrating configurations acquire a finite stationary mean spin-polarization. Of great importance for the chiral induced spin selectivity effect, however, is that the two enantiomers acquire different amplitudes of their spin-polarizations also in the stationary limit.

Here it should be stressed that chiral induced spin selectivity does not originate from the emergence of a spin-polarization in itself, but it is the unequal amplitudes of the spin-polarizations of the enantiomers that form the basis for the phenomenon. This statement can be understood from the following discussion. The chiral induced spin selectivity effect is founded on the difference of the charge currents through a chiral molecule under different conditions. It can, for instance, be electrons photoexcited by circularly polarized light with opposite helicity such that the two photocurrents are dif-

ferent [2]. While there is no question that the environment has a strong effect on the magnetic properties of the molecule, however, unless there is an immanent property of the molecule that responds differently when the light helicity is changed, there cannot be any change in the spin-polarization of the photoelectric current. In this sense, the emergence of the spin-polarization is intimately related to the excited states of the molecule. In the transient regime, these excitations are made available by the dynamical changes of the electronic structure, however, when passing into the stationary regime, those excitations are no longer accessible in the static configuration considered here. That is, in the static configuration there is no mechanism that allows for transferring electron density between states and, in particular, there is no mechanism that sustains an angular momentum transfer within the molecule. Nuclear, or, molecular vibrations, by contrast, facilitate transfer of both electron density and angular momentum between states, or, channels in the molecule. Moreover, at room temperature there is a wide energy window available, about 26 meV, for electrons to transfer between states through thermal excitations, which is a reason for the effectiveness of the nuclear vibrations in this context.

In summary, it has been shown that spin-polarization is dynamically generated in chiral molecules upon interfacing it with a metal. The dynamics indicate that chiral induced spin selectivity is an excited states phenomenon which, in the transient regime is sustained by the strong fluctuations imposed by the temporally changing conditions. When passing over to the stationary regime, the system drives towards a ground state which may be spin-polarized, however, the existence of a non-vanishing spin-polarization depends on whether electronic density and angular momentum can be transferred between the states in the ground state. As has been shown here, nuclear vibrations do allow for such transfer and that these result provide fundamental clues for further development of a comprehensive theory for enantiomer selectivity.

The author thanks R. Naaman for constructive and fruitful discussions. Support from Vetenskapsrådet and Stiftelsen Olle Engkvist Byggmästare is acknowledged.

* Jonas.Fransson@physics.uu.se

- [1] Ray, K.; Ananthavel, S. P.; Waldeck, D. H.; Naaman, R., Asymmetric Scattering of Polarized Electrons by Organized Organic Films of Chiral Molecules, *Science*, **1999**, 283, 814–816.
- [2] Göhler, B.; Hamelbeck, V.; Markus, T. Z.; Kettner, M.; Hanne, G. F.; Vager, Z.; Naaman, R.; Zacharias, H., Spin Selectivity in Electron Transmission Through Self-Assembled Monolayers of Double-Stranded DNA, *Science*, **2010**, 331, 894–897.
- [3] Díaz, E.; Conteras, A.; Hernández, J.; Domínguez-Adame, F., Effective nonlinear model for electron transport in deformable helical molecules, *Phys. Rev. E*, **2018**, 98, 052221.
- [4] Yang, X.; van der Wal, C. H.; van Wees, B. J.; Spin-dependent electron transmission model for chiral molecules in mesoscopic devices, *Phys. Rev. B*, **2019**, 99, 024418.
- [5] Díaz, E.; Albares, P.; Estévez, P. G.; Cerveró, J. M.; Gaul,

- C.; Diez, E.; Domínguez-Adame, F., Spin dynamics in helical molecules with nonlinear interactions, *New J. Phys.*, **2018**, *20*, 043055.
- [6] Michaeli, K.; Naaman, R., Origin of Spin-Dependent Tunneling Through Chiral Molecules, *J. Phys. Chem. C*, **2019**, *123*, 17043–17048.
- [7] Gutierrez, R.; Díaz, E.; Naaman, R.; Cuniberti, G.; Spin-selective transport through helical molecular systems, *Phys. Rev. B*, **2012**, *85*, 081404(R).
- [8] Guo, A. -M.; Sun, Q. -F., Spin-Selective Transport of Electrons in DNA Double Helix, *Phys. Rev. Lett.*, **2012**, *108*, 218102.
- [9] Guo, A. -M.; Sun, A. -F., Spin-dependent electron transport in protein-like single-helical molecules, *Proc. Natl. Acad. Soc.*, **2014**, *111*, 11658–11662.
- [10] Rai, D.; Galperin, M., Electrically Driven Spin Currents in DNA, *J. Phys. Chem. C*, **2013**, *117*, 13730–13737.
- [11] Matityahu, S.; Utsumi, Y.; Aharony, A.; Entin-Wohlman, O.; Balseiro, C. A., Spin-dependent transport through a chiral molecule in the presence of spin-orbit interaction and nonunitary effects, *Phys. Rev. B*, **2016**, *93*, 075407.
- [12] Varela, S.; Mujica, V.; Medina, E., Effective spin-orbit couplings in an analytical tight-binding model of DNA: Spin filtering and chiral spin transport, *Phys. Rev. B*, **2016**, *93*, 155436.
- [13] Behnia, S.; Fathizadeh, S.; Akhshani, A., Modeling spin selectivity in charge transfer across the DNA/Gold interface, *Chem. Phys.*, **2016**, *477*, 61–73.
- [14] Dalum, S.; Hedegård, P., Theory of Chiral Induced Spin Selectivity, *Nano Lett.*, **2019**, *19*, 5253–5259.
- [15] Maslyuk, V. V.; Gutierrez, R.; Dianat, A.; Mujica, V.; Cuniberti, G., Enhanced Magnetoresistance in Chiral Molecular Junctions, *J. Phys. Chem. Lett.*, **2018**, *9*, 5453–5459.
- [16] Díaz, E.; Domínguez-Adame, F.; Gutierrez, R.; Cuniberti, G.; Mujica, V., Thermal Decoherence and Disorder Effects on Chiral-Induced Spin Selectivity, *J. Phys. Chem. Lett.*, **2018**, *9*, 5753–5459.
- [17] Zöllner, M. S.; Varela, S.; Medina, E.; Mujica, V.; Herrmann, C., Insight into the Origin of Chiral-Induced Spin Selectivity from a Symmetry Analysis of Electronic Transmission, *J. Chem. Theory Comput.*, **2020**, *16*, 2914–2929.
- [18] Fransson, J., Chirality-Induced Spin Selectivity: The Role of Electron Correlations, *J. Phys. Chem. Lett.*, **2019**, *10*, 7126–7132.
- [19] Ghazaryan, A.; Lemesko, M.; Volosniev, A. G., Spin Filtering in Multiple Scattering off Point Magnets, *Commun. Phys.*, **2020**, *3*, 178.
- [20] Shitade, A.; Minamitani, E., Geometric Spin-Orbit Coupling and Chirality-Induced Spin Selectivity, *New J. Phys.*, **2020**, *22*, 113023.
- [21] Du, G. -H.; Fu, H. -H.; Wu, R., Vibration-enhanced spin-selective transport of electrons in the DNA double helix, *Phys. Rev. B*, **2020**, *102*, 035431.
- [22] Zhang, L.; Hao, Y.; Qin, W.; Xie, S.; Qu, F., Chiral-induced spin selectivity: A polaron transport model, *Phys. Rev. B*, **2020**, *102*, 214303.
- [23] Fransson, J., Vibrational origin of exchange splitting and chiral induced spin selectivity, *Phys. Rev. B*, **2020**, *102*, 235416.
- [24] Bian, X.; Yanze Wu, Y.; Teh, H. -H.; Zhou, Z.; Subotnik, J. E., Modeling nonadiabatic dynamics with degenerate electronic states, intersystem crossing, and spin separation: A key goal for chemical physics, *J. Chem. Phys.*, **2021**, *154*, 110901.
- [25] Alwan, S.; Dubi, Y., Spinterface Origin for the Chirality-Induced Spin-Selectivity Effect, *J. Am. Chem. Soc.*, **2021**, *143*, 14235–14241.
- [26] Fay, T. P.; Limmer, D. T., Origin of Chirality Induced Spin Selectivity in Photoinduced Electron Transfer, *Nano Lett.*, **2021**, *21*, 6696–6702.
- [27] Hoff, D. A.; Rego, L. G. C., Chirality-Induced Propagation Velocity Asymmetry, *Nano Lett.*, **2021**, *21*, 8190–8196.
- [28] Volosniev, A. G.; Alpern, H.; Paltiel, Y.; Millo, O.; Lemesko, M.; Ghazaryan, A., Interplay between friction and spin-orbit coupling as a source of spin polarization, *Phys. Rev. B*, **2021**, *104*, 024430.
- [29] Dianat, A.; Gutierrez, R.; Alpern, H.; Mujica, V.; Ziv, A.; Yochelis, S.; Millo, O.; Paltiel, Y.; Cuniberti, G., Role of Exchange Interactions in the Magnetic Response and Intermolecular Recognition of Chiral Molecules, *Nano Lett.*, **2020**, *20*, 7077–7086.
- [30] Fransson, J., Charge Redistribution and Spin Polarization Driven by Correlation Induced Electron Exchange in Chiral Molecules, *Nano Lett.*, **2021**, *21*, 3026–3032.
- [31] Mishra, D.; Markus, T. Z.; Naaman, R.; Kettner, M.; Göhler, B.; Zacharias, H.; Friedman, N.; Sheves, M.; Fontanesi, C., Spin-dependent electron transmission through bacteriorhodopsin embedded in purple membrane, *Proc. Natl. Acad. Soc.*, **2013**, *110*, 14872–14876.
- [32] Eckshtain-Levi, M.; Capua, E.; Refaely-Abramson, S.; Sarkar, S.; Gavrilo, Y.; Mathew, S. P.; Paltiel, Y.; Levy, Y.; Kronik, L.; Naaman, R., Cold denaturation induces inversion of dipole and spin transfer in chiral peptide monolayers, *Nat. Comms.*, **2016**, *7*, 10744.
- [33] Fontanesi, C.; Capua, E.; Paltiel, Y.; Waldeck, D. H.; Naaman, R., Spin-Dependent Processes Measured without a Permanent Magnet, *Adv. Mater.*, **2018**, *30*, 1707390.
- [34] Dor, O. B.; Morali, N.; Yochelis, S.; Baczewski, L. T.; Paltiel, Y., Local Light-Induced Magnetization Using Nanodots and Chiral Molecules, *Nano Lett.*, **2014**, *14*, 6042–6049.
- [35] Kettner, M.; Maslyuk, V. V.; Nürenberg, D.; Seibel, J.; Gutierrez, R.; Cuniberti, G.; Ernst, K. -H.; Zacharias, H., Chirality-Dependent Electron Spin Filtering by Molecular Monolayers of Helicenes, *J. Phys. Chem. Lett.*, **2018**, *9*, 2025–2030.
- [36] Xie, Z.; Markus, T. Z.; Cohen, S. R.; Vager, Z.; Gutierrez, R.; Naaman, R., Spin Specific Electron Conduction through DNA Oligomers, *Nano Lett.*, **2011**, *11*, 4652–4655.
- [37] Ghosh, S.; Mishra, S.; Avigad, E.; Bloom, B. P.; Baczewski, L. T.; Yochelis, S.; Paltiel, Y.; Naaman, R.; Waldeck, D. H., Effect of Chiral Molecules on the Electron's Spin Wavefunction at Interfaces, *J. Phys. Chem. Lett.*, **2020**, *11*, 1550–1557.
- [38] Kiran, V.; Mathew, S. P.; Cohen, S. R.; Delgado, I. H.; Lacour, J.; Naaman, R., Helicenes—A New Class of Organic Spin Filter, *Adv. Mater.*, **2016**, *28*, 1957–1962.
- [39] Mondal, A. K.; Brown, N.; Mishra, S.; Makam, P.; Wing, D.; Gilead, S.; Wiesenfeld, Y.; Leitus, G.; Shimon, L. J. W.; Carmieli, R.; Ehre, D.; Kamieniarz, G.; Fransson, J.; Hod, O.; Kronik, L.; Gazit, E.; Naaman, R., Long-Range Spin-Selective Transport in Chiral Metal-Organic Crystals with Temperature-Activated Magnetization, *ACS Nano*, **2020**, *14*, 16624–16633.
- [40] Smolinsky, E. Z. B.; Neubauer, A.; Kumar, A.; Yochelis, S.; Capua, E.; Carmieli, R.; Paltiel, Y.; Naaman, R.; Michaeli, K., Electric Field-Controlled Magnetization in GaAs/AlGaAs Heterostructures-Chiral Organic Molecules Hybrids, *J. Phys. Chem. Lett.*, **2019**, *10*, 1139–1145.
- [41] Dor, O. B.; Yochelis, S.; Mathew, S. P.; Naaman, R.; Paltiel, Y., A chiral-based magnetic memory device without a permanent magnet, *Nat. Comms.*, **2013**, *4*, 2256.
- [42] Dor, O. B.; Yochelis, S.; Radko, A.; Vankayala, K.; Capua, E.; Capua, A.; Yang, S. -H.; Baczewski, L. T.; Parkin, S. S. P.; Naaman, R.; Paltiel, Y., Magnetization switching in ferromagnets by adsorbed chiral molecules without current or external

- magnetic field, *Nat. Comms.*, **2016**, 8, 14567.
- [43] Inui, A.; Aoki, R.; Nishiue, Y.; Shiota, K.; Kousaka, Y.; Shishido, H.; Hirobe, D.; Suda, M.; Ohe, J.; Kishine, J.; Yamamoto, H. M.; Togawa, Y., Chirality-Induced Spin-Polarized State of a Chiral Crystal CrNb_3S_6 , *Phys. Rev. Lett.*, **2021**, 124, 166602.
- [44] Shiota, K.; Inui, A.; Hosaka, Y.; Amano, R.; Ōnuki, Y.; Hedo, M.; Nakama, T.; Hirobe, D.; Ohe, J.; Kishine, J.; Yamamoto, H. M.; Shishido, H.; Togawa, Y., Chirality-Induced Spin Polarization over Macroscopic Distances in Chiral Disilicide Crystals, *Phys. Rev. Lett.*, **2021**, 127, 126602.
- [45] Sukenik, N.; Tassinari, F.; Yochelis, S.; Millo, O.; Baczewski, L. T.; Paltiel, Y., Correlation between Ferromagnetic Layer Easy Axis and the Tilt Angle of Self Assembled Chiral Molecules, *Molecules*, **2020**, 25, 6036.
- [46] Kumar, A.; Capua, E.; Kesharwani, M. K.; Martin, J. M. L.; Sitbon, E.; Waldeck, D. H.; Naaman, R., Chirality-induced spin polarization places symmetry constraints on biomolecular interactions, *Proc. Natl. Acad. Soc.* **2017**, 114, 2474–2478.
- [47] H. Alpern, K. Yavilberg, T. Dvir, N. Sukenik, M. Klang, S. Yochelis, H. Cohen, E. Grosfeld, H. Steinberg, Y. Paltiel, and O. Millo, Magnetic-related State and Order Parameter Induced in a Conventional Superconductor by Nonmagnetic Chiral Molecules, *Nano Lett.*, **2019**, 19, 5167–5175.
- [48] H. Shiba, Classical Spins in Superconductors, *Prog. Theor. Phys.*, **1968**, 40, 435–451.
- [49] L. Yu, Bound State in Superconductors with Paramagnetic Impurities, *Acta Phys. Sin.*, **1965**, 21, 75–91.
- [50] A. Rusinov, Superconductivity near a Paramagnetic Impurity, *JETP Lett.*, **1969**, 9, 85–87.
- [51] Banerjee-Ghosh, K.; Dor, O. B.; Tassinari, F.; Capua, E.; Yochelis, S.; Capua, A.; Yang, S. -H.; Parkin, S. S. P.; Sarkar, S.; Kronik, L.; Baczewski, L. T.; Naaman, R.; Paltiel, Y., Separation of enantiomers by their enantiospecific interaction with achiral magnetic substrates, *Science*, **2018**, 360, 1331–1334.
- [52] Naaman, R.; Waldeck, D. H.; Paltiel, Y., Chiral molecules-ferromagnetic interfaces, an approach towards spin controlled interactions, *Appl. Phys. Lett.*, **2019**, 115, 133701–133704.
- [53] Santra, K.; Zhang, Q.; Tassinari, F.; Naaman, R., Electric-Field-Enhanced Adsorption of Chiral Molecules on Ferromagnetic Substrates, *J. Phys. Chem. B*, **2019**, 123, 9443–9448.
- [54] Ziv, A.; Saha, A.; Alpern, H.; Sukenik, N.; Baczewski, L. T.; Yochelis, S.; Reches, M.; Paltiel, Y., AFM-Based Spin-Exchange Microscopy Using Chiral Molecules, *Adv. Mater.*, **2019**, 31, 1904206–1904212.
- [55] Santra, K.; Bhowmick, D.; Zhu, Q.; Bendikov, T.; Naaman, R., A Method for Separating Chiral Enantiomers by Enantiospecific Interaction with Ferromagnetic Substrates, *J. Phys. Chem. C*, **2021**, 125, 17530–17536.
- [56] Metzger, T. S.; Siam, R.; Kolodny, Y.; Goren, N.; Sukenik, N.; Yochelis, S.; Abu-Reziq, R.; Avnir, D.; Paltiel, Y., Dynamic Spin-Controlled Enantioselective Catalytic Chiral Reactions, *J. Phys. Chem. Lett.*, **2021**, 12, 5469–5472.
- [57] Jauho, A. -P.; Wingreen, N. S.; Meir, Y., Time-dependent transport in interacting and noninteracting resonant-tunneling systems, *Phys. Rev. B*, **1994**, 50, 5528–5544.
- [58] Wang, C.; Guo, A. -M.; Sun, Q. -F.; Yan, Y., Efficient Spin-Dependent Charge Transmission and Improved Enantioselective Discrimination Capability in Self-Assembled Chiral Coordinated Monolayers, *J. Phys. Chem. Lett.*, **2021**, 12, 10262–10269.